Femtosecond Fiber Laser Based on $BiSbTeSe_2$ Quaternary Material Saturable Absorber

Yue-Jia Xiao(肖悦嘉)[1], Xiao-Wei Xing(邢笑伟)[1], Wen-Wen Cui(崔文文)[1], Yue-Qian Chen(陈悦芊)[1], Qin Zhou(周勤)[2], and Wen-Jun Liu(刘文军)[1*]

[1]*State Key Laboratory of Information Photonics and Optical Communications, School of Science, Beijing University of Posts and Telecommunications, Beijing 100876, China*
[2]*School of Mathematical and Physical Sciences, Wuhan Textile University, Wuhan 430200, China*

(Received 13 February 2023; accepted manuscript online 30 March 2023)

Topological insulator materials, including Bi_2Te_3, Sb_2Te_3, Sb_2Te_3, and Bi_2Se_3, have attracted some attention due to their narrow band gaps, high carrier mobility, wide spectral absorption ranges and other characteristics. We report a new multi-compound topological insulator material $BiSbTeSe_2$ that, compared with the traditional topological insulator composed of two elements, can integrate the physical advantages of each element, helpful to build an experimental platform with rich physical properties. The nonlinear optical characteristics of the quaternary material $BiSbTeSe_2$ is obtained in the erbium-doped fiber laser. Using the $BiSbTeSe_2$ as a saturable absorber material, the passive Q-switched and mode-locked fiber lasers are achieved. The pulse duration and signal-to-noise ratio (SNR) of the Q-switched fiber laser are 854 ns and 70 dB, respectively. Meanwhile, the pulse duration and SNR of the mode-locked fiber laser are 259 fs and 87.75 dB, respectively. This work proves that the $BiSbTeSe_2$ has a considerable application prospect as a saturable absorber in fiber lasers, and provides a new reference for selection of high-performance saturable absorber materials.

DOI: 10.1088/0256-307X/40/5/054201

In recent years, with the acquisition of some representative applications in the fields of environmental sensing, integrated circuits, communications and medical treatment, research value of ultrafast lasers is gradually increasing.[1–7] As a representative of ultrafast lasers, passive mode-locked fiber lasers based on saturable absorbers have advantages such as low pump threshold, wide wavelength range, short recovery time, simple preparation, flexible and compact design, and easy fiber integration and compatibility. At the same time, mode-locked fiber lasers are popular because of their long operating life and high stability.[8–12] The mode-locking technology of the fiber laser is not single. The laser based on the passive mode-locking technology has gradually become a hot topic in recent years because it does not need additional active control devices, and has the advantages of the high signal-to-noise ratio (SNR) and narrow pulse duration.[13–15] For ultrafast lasers, choice of gain medium is not exactly the same. Erbium-doped fiber (EDF) lasers are widely used in ultrafast lasers because of their strong stability, favorable laser quality, low laser threshold, and high conversion efficiency. EDF lasers are mainly used in space optical communication, industrial processing, laser radar, and other fields, and are expected to replace other types of fiber lasers in fiber communications.[16–18]

At present, lasers based on semiconductor saturable absorption mirrors (SESAMs) occupy a large share in the market of fiber lasers, and the research on SESAM has been gradually improved.[19–24] However, due to high prices of SESAMs, replacement of SESAMs has been discussed. The search for alternatives to SESAMs has opened a new avenue by focusing on excellent optical properties of nanomaterials. The optical core device that replaces SESAMs in the passive mode-locking technology is saturable absorbers (SAs),[25–27] which is a new generation of key optical devices based on nanomaterials. The SA materials mainly rely on graphene,[28,29] black phosphorus,[30,31] transition metal sulfide,[32,33] and topological insulator (TI),[34,35] etc. Those materials have the application prospects in the field of nonlinear optics.

Among them, TIs have exhibited highly conducting and massless spin-helical surface states on their surface. Those unique characteristics are caused by combination of spin-orbit interaction and time-reversal symmetry, which also lead to the excellent optical performance of prepared SAs, which lays a prerequisite for the preparation of efficient SAs.[36] At the same time, compared with other types of materials, TIs have the advantages of the wide spectral absorption range, high carrier mobility, narrow band gap, and so on,[36–38] which have their own advantages in selection of SA preparation materials, and also bring new development opportunities to improvement of performance of photoelectric devices.

However, small band gap structures of TIs are difficult to achieve in experiment.[39,40] With the CdTe/HgTe/CdTe quantum well model first proposed, TIs have been successfully prepared,[41,42] the feasibility and excellence of the TIs were proved, and research of those kinds of materials was opened. In a typical TI, the pulse duration of the mode-locked laser based on the Sb_2Se_3-SA could reach 890 fs, and the SNR was 57 dB.[43] The output of the Q-switched pulse was obtained based on the Bi_2Te_3-SA, and the mode-locked pulse was realized by combining with the $FeTe_2$ material, the pulse duration

*Corresponding author. Email: jungliu@bupt.edu.cn
© 2023 Chinese Physical Society and IOP Publishing Ltd

was narrowed to 481 fs, and the SNR was 55 dB.[44] Most of the TI materials which have been studied are binary materials with relatively low SNR and wide pulse duration. As a novel quaternary TI material, the $BiSbTeSe_2$ has obtained some interesting results in recent years due to its strong spin-orbit coupling effect and stable energy gap.[45–47] Some studies have shown that the band gap of the $BiSbTeSe_2$ is 0.25 eV,[48] and the carrier density can reach $10^{12}\,cm^{-2}$.[49] At the same time, German *et al.* have shown that the $BiSbTeSe_2$ is one of the most bulk-insulating three-dimensional TIs,[50] which makes it important in the TI research. This research also shows the potential application of this material in the field of optical devices. However, the possibility of the $BiSbTeSe_2$ as a modulator in passively mode-locked fiber lasers and the related nonlinear optical characteristics are not explored. Although some polarization-dependent losses are generated during the experiment, the combination of materials maintains the excellent properties of the TI materials, improves the SNR of the output pulse, and shortens the pulse duration. Therefore, the application potential of this TI material in nonlinear optics is explored in this Letter.

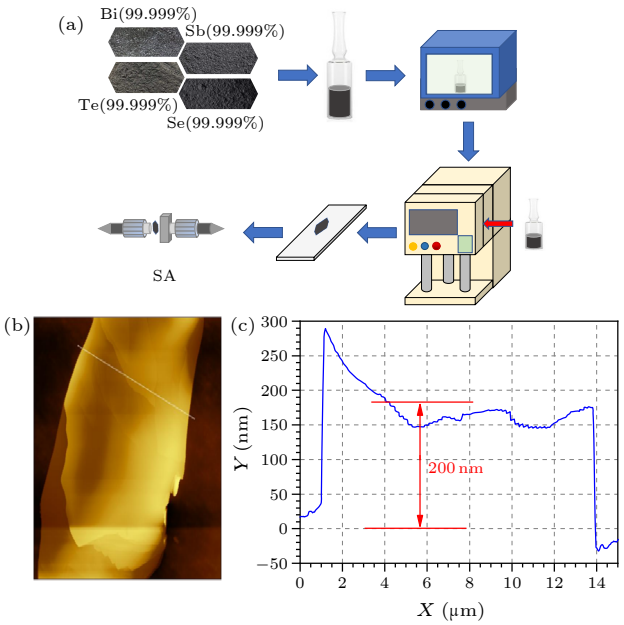

Fig. 1. (a) Preparation process of the $BiSbTeSe_2$-SA. (b) AFM images of 200 nm-$BiSbTeSe_2$ films. (c) Material thickness curve.

Material Preparation. A two-step method was used for obtaining $BiSbTeSe_2$ single crystals. Firstly, stoichiometric ratio of Bi (99.999%, Alfa Aesar), Sb (99.999%, Alfa Aesar), Te (99.999%, Alfa Aesar) and Se (99.999%, Alfa Aesar) shots were sealed into ampoule. The ampoule was kept at 850℃ for 48 h with shaking about 20 times and followed by slow cooling in a box furnace. Secondly, the ampoule was put into a two-zone Bridgeman furnace in which upper temperature and lower temperature were set at 720℃ and 550℃, respectively. The dropping approaching speed of the ampoule was 1 mm/h. Finally, the high-quality single crystal of $BiSbTeSe_2$ were obtained.

In order to further explore the optical properties of the $BiSiTeSe_2$ materials in fiber lasers, the mechanical exfoliation (ME) method was used to obtain material films from the $BiSbTeSe_2$ crystals. The ME preparation process has the advantages of the simple operation, smooth material surface, and high mobility. Polydimethylsiloxane (PDMS) was used to cover and peel the material, and the film of $BiSbTeSe_2$ was finally attached to the PDMS, as shown in Fig. 1(a). Because of the material film preparation method adopted, the measurement of atomic force microscopy (AFM) image is the most intuitive and easy to implement, after the preparation of the $BiSiTeSe_2$ material film, AFM was used to measure the thickness of the film and to observe the surface morphology of the material. The characterization diagram of the material film is shown in Fig. 1(b). The thickness curve of the material obtained by the probe measurement is shown in Fig. 1(c). According to the figure, the average thickness of the $BiSiTeSe_2$ is about 200 nm, and its surface is relatively flat. After measuring the thickness of the material film, it is transferred to the end face of the fiber optic patch cable to make an SA. There are three merging options for the preparation of SAs, which are embedded, reflective and tapered fibers. Since the $BiSbTeSe_2$ crystal is a TI material, in order to better prevent topological phase transition of the material and to provide better saturation absorption, the preparation method of the embedded SA was selected in this experiment.

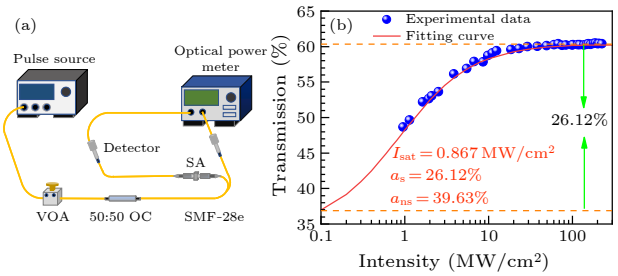

Fig. 2. Nonlinear optical characterization of the $BiSbTeSe_2$-SA. (a) Balanced two-arm detector device. (b) Modulation depth curve of 200 nm $BiSbTeSe_2$ film.

In order to explore the saturation absorption characteristics of the $BiSbTeSe_2$ material, the balanced twin-detector device method was used for measurement. The experimental setup is shown in Fig. 2(a). The principle of this method is to divide the mode-locked pulse output of femtosecond laser into two beams with the same intensity through optical coupler (OC), and the division ratio is 50 : 50. One part is directly connected to the power meter as a reference beam, and the other part passes through the sample to be measured by the power meter. The ratio of light intensity detected by the two outputs can reflect the modulation depth of the SA. The operating wavelength of the laser source used in the measurement experiment is 1550 nm, the shortest pulse duration and repetition rate are 185 fs and 73 MHz, respectively. By changing the input light intensity in the optical path with a variable optical attenuator (VOA), a series of corresponding stable average power at the two output ends can be obtained. The following function is used to fit the measured data to obtain the modulation depth of the material:

$$\alpha(I) = \frac{\alpha_s}{1 + I/I_{sat}} + \alpha_{ns}, \tag{1}$$

where α_s represents the modulation depth of $BiSbTeSe_2$ film, α_{ns} represents the nonsaturable loss which means the absorption of the laser in addition to the saturation absorption. I_{sat} in the function is the saturation intensity of the fiber laser. The fitting results are shown in Fig. 2(b). The modulation depth, saturation strength, and unsaturated loss of the material with a thickness of 200 nm are 26.12%, 0.867 MW/cm^2, and 39.63%, respectively.

Experimental Setup. In order to observe the nonlinear optical properties of the $BiSbTeSe_2$-SA, an experimental device based on EDF laser is built. The length of the resonator of the experimental optical path is 4.02 m. The structure of the fiber laser is shown in Fig. 3. The resonator cavity mainly contains the following optical components: a pump source (LD) with central wavelength and maximum output power of 976 nm and 630 mW is used to provide energy; a 980/1550 nm wavelength division multiplexer (WDM) is used for beam integration of different wavelengths; EDF (Liekki110-4/125) with a length of 33 cm is used for optical pulse amplification; an optical coupler (OC) with the optical ratio of 80 : 20 is used to realize the real-time detection of pulses, and the output femtosecond pulses is exported at the 20% output port during the experiment.

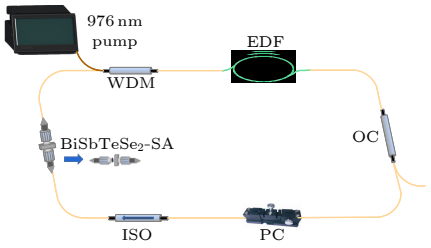

Fig. 3. Experimental setup of EDF laser based on the $BiSbTeSe_2$.

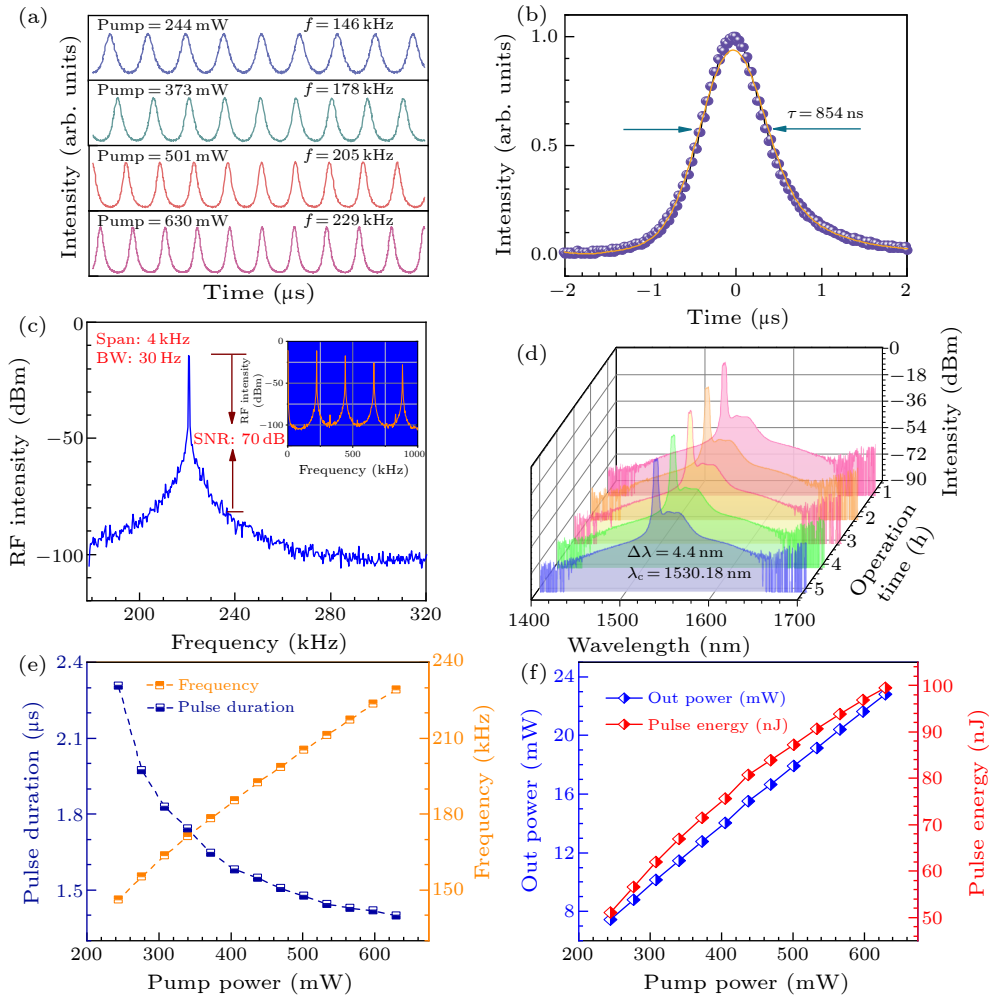

Fig. 4. Output characterization of 200 nm $BiSbTeSe_2$-SA Q-switched laser. (a) Pulse distribution. (b) Q-switched pulse duration. (c) Radio frequency (RF) spectrum. (d) Pulse spectrum. (e) The pulse duration and repetition rate. (f) Trend curves of output power and single pulse energy.

At the same time, in order to obtain the best performance of femtosecond laser pulses by adjusting the polarization state in the cavity, a polarization controller (PC) is added after the OC for adjustment. Because it is necessary to control the light beam in the cavity to only propagate in one direction, an isolator (ISO) is added into the cavity to ensure the light propagation direction and to improve the light transmission efficiency. Finally, the $BiSbTeSe_2$-SA with a material thickness of 200 nm is added to the loop for the corresponding optical performance test. The

group velocity dispersion (GVD) of the EDF at 1550 nm is 12 ps^2/km, and the net dispersion is estimated to be $-0.08091\ ps^2$, which allows conventional soliton formed in the fiber laser. The measurement of the specific parameters of the optical pulse is completed by the following equipment: continuous detection and recording of the pulse sequence is finished by an oscilloscope (Tektronix DPO 3054), measurement of the pulse duration is finished by an autocorrelator (APE Pulse check), RF spectrum analyzer (Rohde & Schwarz FSW26) is used to measure the pulse SNR, and finally a spectrum analyzer (Yoko-gawa AQ 6370 C) is used to observe and record the optical spectrum of the output light.

Results and Discussion. The $BiSbTeSe_2$-SA device is tested under the condition that the total resonator cavity length is 4.02 m. In the process of adjusting the pump power, it is found that the threshold of the Q-switched pulse is 202.5 mW. With the increase of pumping power, the fiber laser can always maintain a stable Q-switched waveform output, and it is found that the repetition frequency is positively correlated with pumping power, as shown in Fig. 4(a). When the pump power is increased to 630 mW, the output single pulse pattern is captured by an oscilloscope, and the shortest pulse duration can be measured to be 854 ns, as shown in Fig. 4(b). In the meantime, the spectrum analyzer is used to observe the spectrum of the output pulse, and it is found that the repetition frequency is 229 kHz and the SNR is 70 dB, in the process of calculating the SNR, the most stable part is marked as the signal. The spectrum diagram of the pulse is shown in Fig. 4(c), which also proves that the Q-switched state at this time is relatively stable. In addition, the spectral analyzer is used to detect the optical spectrum of the pulse every hour for five consecutive hours, and it is found that the spectrum always remains stable, as shown in Fig. 4(d). According to the spectrum, the central wavelength of the laser is 1530.18 nm, and the spectral bandwidth is 4.40 nm. The pulse duration and repetition frequency of the Q-switched laser output pulse are closely related to its power. By adjusting the output power of the pump source, it is found that with the increase of the pump power, the repetition frequency of the laser increases and the pulse duration decreases. The change curve is shown in Fig. 4(e). When the pump power is 630 mW, the maximum output power of the laser can reach 22.81 mW, and the corresponding single pulse energy is calculated to be up to 99.5 nJ. At the same time, it is found that the changes of the optical pulse output power and the single pulse energy are consistent with the change trend of the pump power, as shown in Fig. 4(f), the single pulse energy is based on the quotient of output power and repetition frequency at the same pump power.

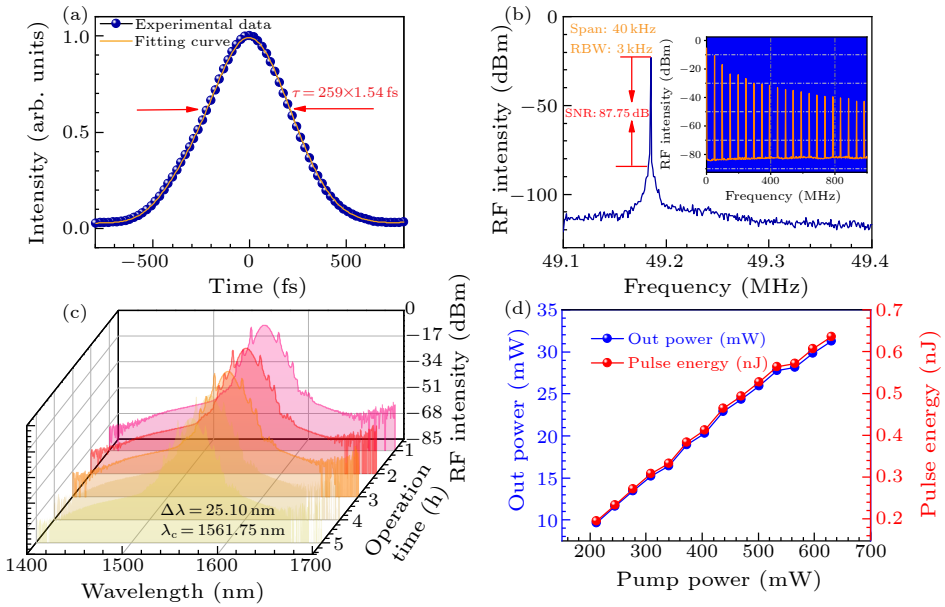

Fig. 5. Output characterization of 200 nm $BiSbTeSe_2$-SA mode-locked laser. (a) Pulse duration. (b) RF spectrum. (c) Pulse spectrum. (d) Trend curves of output power and pulse energy.

Without changing the length of the resonator, the SA device and other components used, the laser can reach the mode-locked state by changing the polarization state in the cavity. After some attempts, it is found that the laser can always output stable mode-locked waveform and ensure a good working state. When the pump power is increasing, the continuous waveform sequence can always be observed on the oscilloscope. The output pulse duration under the mode-locked state is accurately measured at the output end of the laser using an autocorrelator. After fitting the $sech^2$ curve, the single pulse duration is 259 fs, which almost conforms the hyperbolic secant distribution in Fig. 5(a). Figure 5(b) shows the output pulse spectrum obtained when the sweep width is 40 kHz and the resolution bandwidth is 3 kHz. It is found that the output SNR is as high as 87.75 dB, which is a better performance than the other laser based on TI materials. Figure 5(c) shows the spectral image of the mode-locked pulse, five spectral images are measured sequentially within five consecutive hours at equal time intervals. The central wavelength of each spectrum is 1561.75 nm, and the pulse bandwidth is 25.1 nm, which prove the working stability of the

mode-locked laser. When exploring the stability and power change of the mode-locked laser, it is found that the mode-locking threshold is 190 mW by constantly adjusting the pump power, and the highest output power of 32.28 mW is reached when the pump power is 630 mW. The relationship among the output power, single pulse energy, and pump power is shown in Fig. 5(d), and the change trend is still consistent.

The Q-switched EDF laser and mode-locked EDF laser based on the $BiSbTeSe_2$-SA are implemented, and their central wavelength is in the range of 1550 nm band, which has a broad application prospect. To more accurately explore the optical properties of the SA components and to reduce the influence of other factors on the laser performance, only the all-fiber EDF lasers are compared, and the comparison results are shown in Table 1, which are compared with fiber lasers based on different TIs-SA. Other TIs for comparison have elements similar to the $BiSbTeSe_2$, but they are generally binary materials. When Bi, Sb, Te, and Se element are combined into quaternary materials, it is found that the laser in this work has excellent performance in the pulse duration, SNR and output power. Due to the higher material band gap and stronger insulation of the $BiSbTeSe_2$, it has the strong ability to absorb the weak light, which can well optimize the waveform along the front edge and back edge of the pulse. At the same time, the shorter length of the fiber laser can reduce the noise signal, which may lead to a certain improvement of the SNR of the laser.

Table 1. Performance comparison with mode-locked fiber lasers based on different SAs.

Material type	Modulation depth	Pulse duration (fs)	SNR (dB)	Output power (mW)	References
PMMA-Bi_2Te_3		505	67.7		[36]
Bi_2Te_3-$FeTe_2$	54%	481	55	6.257	[44]
Sb_2Te_3	6%	270	70	1	[51]
Bi_2Te_3	15.7%	600	65	0.8	[52]
Bi_2Se_3	5.2%	360	56	0.86	[53]
$BiSbTeSe_2$	26.12%	259	87.75	32.28	This work

In summary, we have verified the possibility of the $BiSbTeSe_2$ as an SA material working in fiber lasers. The $BiSbTeSe_2$ with a thickness of 200 nm has been obtained by melting and mechanical stripping, and it has been added as an optical modulator to an EDF laser to explore its nonlinear optical performance. The $BiSbTeSe_2$-SA laser has successfully achieved the Q-switching and mode-locking outputs at the same cavity length. The shortest pulse duration of the Q-switched laser is 854 ns, the SNR is 70 dB, and the maximum output power is 22.81 mW. In addition, the performance of the $BiSbTeSe_2$ in the mode-locked lasers is superior, which can generate laser pulses with a pulse duration of only 259 fs, an SNR of 87.75 dB, and output power of more than 30 mW. It has been found that the laser based on the $BiSbTeSe_2$-SA has excellent performance. This work has indicated that composite materials can further improve the relevant optical properties, and provide more choices for the preparation of SA in the future.

Acknowledgement. This work was supported by the Beijing Natural Science Foundation (Grant No. JQ21019), and the National Natural Science Foundation of China (Grant Nos. 12075034 and 11974003).

References

[1] Liu Z J, Jin X X, Su R T, Ma P F, and Zhou P 2019 *Sci. Chin. Inf. Sci.* **62** 41301
[2] Maria H, Jasper P, Marius P, Hugo D, Kévin V, Eric C, Peter S, Hampus W, Sylvain M, Chen G, Cord A, Anne L H, and Johnsson E 2021 *Ultrafast Sci.* **2021** 9797453
[3] Gong Q H and Zhao W 2021 *Ultrafast Sci.* **2021** 9765859
[4] Huang Y D, Zhao J, Shu Z, Zhu Y L, Liu J L, Dong W P, Wang X W, Lv Z H, Zhang D W, Yuan J M, Chen J, and Zhao Z X 2021 *Ultrafast Sci.* **2021** 9837107
[5] Boolakee T, Heide C, Garzón-Ramírez A *et al.* 2022 *Nature* **605** 251
[6] Yuki K, Christian H, Koochaki K M, Amalya J, Liu F, Heinz T F, and David A 2021 *Ultrafast Sci.* **2021** 9820716
[7] Zervas M N and Codemard C A 2014 *IEEE J. Sel. Top. Quantum Electron.* **20** 0904123
[8] Ahmad H, Hidayah M N, Aisyah R S, Muhamad Z S, Muhammad U M I, and Norazriena Y 2022 *Opt. Fiber Technol.* **73** 103013
[9] Ahmad H, Kahar N H A, Yusoff N, Hanafi A I M, Ramli R, Harun S W, and Reduan S A 2022 *Opt. Laser Technol.* **155** 108397
[10] Liu J T, Yang F, Lu J P, Ye S, Guo H W, Nie H K, Zhang J L, He J L, Zhang B T, and Ni Z H 2022 *Nat. Commun.* **13** 3855
[11] Liu W J, Pang L H, Han H N, Liu M L, Lei M, Fang S B, Teng H, and Wei Z Y 2017 *Opt. Express* **25** 2950
[12] Yuan M Y, Wang W Q, Wang X Y, Wang Y, Yang Q H, Cheng D, Liu Y, Huang L, Zhang M G, Liang B, Zhao W, and Zhang W F 2021 *Opt. Lett.* **46** 4855
[13] Leke P A and Dikandé A M 2020 *Appl. Phys. B* **126** 157
[14] Li L J, Zhou L, Li T X, Yang X N, Xie W Q, Duan X M, Shen Y J, Yang Y Q, Yang W L, and Zhang H 2020 *Opt. Laser Technol.* **124** 105986
[15] Liu W J, Pang L H, Han H N, Bi K, Lei M, and Wei Z Y 2017 *Nanoscale* **9** 5806
[16] Carlos M J 2022 *Opt. Commun.* **525** 128856
[17] Zhao L, Xu N N, Shang X X, Liu X Y, Huang P, Lu H, Zhang H N, and Li D W 2022 *Laser Phys.* **32** 095101
[18] Yusoff N M, Abdul H M A W, Zainol A N H, Alresheedi M T, Goh C S, and Mahdi M A 2022 *Optik* **257** 168730
[19] Armas R I, Rodriguez M L A, Durán-Sánchez M, Avazpour M, Carrascosa A, Silvestre E, Kuzin E A, Andrés M V, and Ibarra-Escamilla B 2021 *Opt. Laser Technol.* **134** 106593
[20] Dai S G, Li X, Wu D D, and Nie Q H 2018 *Optik* **165** 195
[21] Mashiko Y, Fujita E, Tokurakawa M 2016 *Opt. Express* **24** 26515
[22] Afifi G, Khedr M A, Badr Y, Danailov M, Sigalotti P, Cinquegrana P, Alsou M B, and Galaly A R 2016 *Opt. Fiber Technol.* **29** 74
[23] Song R, Chen H W, Chen S P, Hou J, and Lu Q S 2011 *J. Opt.* **13** 035201
[24] Luo Z C, Luo A P, and Xu W C 2011 *IEEE Photon. J.* **3** 64
[25] Kaur N J and Soumendu J 2022 *Chaos Soliton. Fract.* **158** 111983
[26] Xiong Z D, Jiang L L, Cheng T T, and Jiang H H 2022 *Infrared Phys. Technol.* **122** 104087
[27] Lau K Y, Zheng J C, Jin C, and Yang S 2022 *Infrared Phys. Technol.* **122** 104103

[28] Baylam I, Cizmeciyan M N, Kakenov N, Kocabas C, and Sennaroglu A 2019 *2D Mater.* **6** 035013
[29] Lee H, Kwon W S, Kim J H, Kang D, and Kim S 2015 *Opt. Express* **23** 22116
[30] Markom A M, Tan S J, Muhammad A R, Paul M C, Dhar A, Das S, Latiff A A, and Harun S W 2020 *Optik* **223** 165635
[31] Pawliszewska M, Ge Y Q, Li Z J, Zhang H, and Sotor J 2017 *Opt. Express* **25** 16916
[32] Li L, Lv R D, Liu S C, Wang X, Wang Y G, Chen Z D, and Wang J 2018 *Laser Phys.* **28** 055106
[33] Ahmad H, Kahar N H A, Yusoff N, Samion M Z, Reduan S A, Ismail M F, Bayang L, Wang Y, Wang S Y, and Sahu J K 2022 *Opt. Fiber Technol.* **69** 102851
[34] Yang J N, Li Y H, Tian K, Liu F F, Dou X D, Ma Y J, Han W J, Xu H H, and Liu J H 2018 *Laser Phys. Lett.* **15** 125802
[35] Al-Masoodi A H H, Ahmad F, Ahmed M H M, Al-Masoodi A H H, Alani I A M, Arof H, and Harun S W 2018 *IET Optoelectron.* **12** 180
[36] Jiang G B, Zhou Y, Wang L L, and Chen Y 2018 *Adv. Cond. Matter Phys.* **2018** 7578050
[37] Zhang X, Wang J, and Zhang S C 2010 *Phys. Rev. B* **82** 245107
[38] Tian W C, Yu W B, Shi J, and Wang Y K 2017 *Materials* **10** 814
[39] Haris H, Muhammad A R, Tan S J, Markom A M, Harun S W, Megat H M M I, and Saad I 2022 *Infrared Phys. Technol.* **123** 104154
[40] Fukui T and Hatsugai Y 2007 *Phys. Rev. B* **75** 121403
[41] Kane C L and Mele E J 2005 *Phys. Rev. Lett.* **95** 226801
[42] Bernevig B A, Hughes T L, and Zhang S C 2006 *Science* **314** 1757
[43] Ma X H, Chen W, Tong L, Liu S Q, Dai W W, Ye S S, Zheng Z Q, Wang Y Y, Zhou Y, Zhang W, Fang W T, Chen X L, Liao M S, and Gao W Q 2021 *Opt. Laser Technol.* **143** 107286
[44] Zhang L F, Liu J F, Li J Z, Wang Z, Wang Y G, Ge Y W, Dong W L, Xu N, He T C, Zhang H, and Zhang W J 2020 *Laser Photon. Rev.* **14** 1900409
[45] Jiang Y J, Li S S, Zhu P, Zhao J G, Xiong X L, Wu Y T, Zhang X, Li Y K, Song T L, Xiao W D, Wang Z W, and Han J F 2022 *J. Appl. Biomater. Func.* **5** 1084
[46] Brevoord J M, Wielens D, Lankhorst M, Díez-Mérida J, Huang Y K, Li C, B, and Brinkman A 2021 *Nanotechnology* **32** 435001
[47] Kaveev A K, Suturin S M, Golyashov V A, Kokh K A, and Tereshchenko O E 2019 *J. Phys. Conf. Ser.* **1400** 055016
[48] Knispel T, Jolie W, Borgwardt N, Lux J, Wang Z W, Ando Y, Rosch A, Michely T, and Grüninger M 2017 *Phys. Rev. B* **96** 195135
[49] Wang J M, Kurzendorfer A, Chen L, Wang Z W, Ando Y, Xu Y, Miotkowski I, Chen Y P, and Weiss D 2021 *Appl. Phys. Lett.* **118** 253107
[50] German R, Komleva E V, Stein P, Mazurenko V G, Wang Z W, Streltsov S V, Ando Y, and van Loosdrecht P H M 2019 *Phys. Rev. Mater.* **3** 054204
[51] Sotor J, Sobon G, Grodecki K, and Abramski K M 2014 *Appl. Phys. Lett.* **104** 251112
[52] Lee J, Koo J, Jhon Y M, and Lee J H 2014 *Opt. Express* **22** 6165
[53] Li K X, Song Y R, Yu Z H, Xu R Q, Dou Z Y, and Tian J R 2015 *Laser Phys. Lett.* **12** 105103